LABORATORY MEASUREMENTS OF THE VORTEX-INDUCED VIBRATIONS OF AN UNTENSIONED CATENARY RISER WITH HIGH CURVATURE

J R Chaplin and R King
Faculty of Engineering and the Environment
University of Southampton UK

ABSTRACT

Measurements of the vortex-induced vibrations of an instrumented catenary model riser with high curvature and very low bending stiffness are presented and discussed. The riser had a diameter of 56mm and a length of 5.36m. It was tensioned only by its own weight and by drag and was tested in a recirculating water channel 2m deep at flow speeds up to 1.4m/s in both directions, i.e. with the upstream anchorage on the floor of the tank and the downstream one at the surface (defined as positive current cases), and then vice versa (negative currents). In many cases much of the riser rested on the tank floor with the touch-down point determined by the flow-induced forces on it. Attention is focused mainly on the frequencies of cross-flow vibrations after careful analysis of the effects of gravitational contamination on acceleration measurements. Response spectra were found to have a higher bandwidth than those of tensioned risers perpendicular to the flow and often exhibited more than one distinct peak. Dimensionless peak frequencies (having been normalised with respect to the diameter and a characteristic velocity) were much lower than that associated with a Strouhal number in the region of 0.2. In positive currents (based on the normal incident velocity at the top of the riser, where it was near vertical) it was generally uniform over the length of the riser at about 0.11. In negative currents, away from the tank floor, the riser's profile was a straight line whose inclination was such that the normal incident velocity was independent of the current speed when this exceeded about 0.5m/s. In these conditions the dimensionless peak frequency (based on the uniform normal incident velocity) was about 0.13.

1. INTRODUCTION

Vortex-induced vibrations of risers have been studied mainly with reference to those that do not undergo large displacements from a straight line, are aligned at right angles to the flow, and are not subject to large variations of tension over their length, or indeed of variations of their effective length. Laboratory measurements made under these conditions, reported by Chaplin et al. (2005), Trim et al. (2005), Huera-Huarte and Bearman (2009) Gu et al. (2013) and others, are characterised by responses often in well-defined structural modes, and at well-defined frequencies in the range $0.16U/d$ to $0.18U/d$ (with diameter d and flow velocity U). The results of these experiments have supported significant developments in the validation of numerical models aimed at the problem of predicting fatigue damage of deep water risers offshore. But when it comes to catenary risers, umbilicals and marine cables that have large curvature, are inclined at various angles to the flow, and experience significant changes in tension over their length, understanding of vortex-induced vibrations is much less well advanced. Related basic problems that have been studied experimentally or numerically include vortex shedding from yawed cylinders (King, 1977; Ramberg, 1983), vibrations of spring-mounted rigid cylinders, or of flexible cylinders, in yawed or sheared flow (Jain and Modarres-Sadeghi, 2013), the wake dynamics and vibrations of rigid cylinders whose axis is curved (strictly 'pipes': Miliou et al., 2007), and interactions at the touch-down point on a hard or a soft sea floor (Kim et al. (2006), Wang et al. (2015b)). Dynamics of catenary risers driven by vessel motions in

initially still water have been studied by Chatjigeorgiou et al. (2008), Pereira et al. (2013) and Wang et al. (2015a).

This paper is concerned with laboratory measurements of the vortex-induced vibrations of a very flexible model riser, 56mm diameter, 5.36m long, in steady currents. In still water the riser hung in a catenary, nearly vertical at the top, with some portion of it resting on the floor of the tank at the bottom. Typical radii of curvature were a metre or less. Accounts of previous comparable experiments are provided by Morooka and Tsukada (2013) and Fan et al. (2015). In Morooka and Tsukada's case the riser had a diameter of 8mm and a length of 5.2m, and was towed through still water 3.6m deep at speeds of up to 0.07m/s. Vibrations of the riser were recorded by means of pairs of accelerometers at four points over its length. Inferred amplitudes of cross-flow displacements (possibly subject to the effects of the gravitational contamination discussed below) rarely exceeded one diameter, while maximum in-line displacements were about one-fifth of this. Morooka and Tsukada identified 'power-in' regions where the expected vortex shedding frequencies based on the normal component of the velocity were within range of computed modal frequencies of the structure. They were able to show that vibrations elsewhere along the riser could be linked to travelling waves that originated in these regions, giving rise to quite closely spaced peaks in spectra of accelerations.

In experiments by Fan et al. (2015) the riser was 20mm in diameter, 7.8m long, and was suspended in water 6m deep of which the current occupied just the top 1.2m, the rest of the water column being initially stationary. The results focus on measurements of bending strain at six points, three in the current and three around the bend at the bottom. Spectra of strains revealed increases in peak frequency with flow speed, and again generally have more than one peak.

In both these experiments, by Morooka and Tsukada (2013) and Fan et al. (2015), the lower anchorage was upstream of the upper one, and the shape of the riser could be said to be concave to the oncoming current. An idealised example of this situation, in which the axis of the (stationary) cylinder traces out just one quarter of a circle with one end pointing directly upstream was studied numerically by Miliou et al. (2007) at Reynolds numbers of 100 and 500. They also computed the convex case, in which one end of the curved cylinder points downstream. The patterns of vortex shedding in the two configurations were radically different. In the concave case vortex shedding was completely suppressed at a Reynolds number of 100, but in a mild form at Re = 500 it was apparently driven primarily by shedding at that part of the cylinder which was normal to the incident flow. However, its frequency, corresponding to a Strouhal number of 0.11, was considerably lower than those for the convex case and much lower than that for a straight cylinder at the same Reynolds number.

Assi et al. (2014) describe measurements of the vibrations of a spring-mounted rigid curved cylinder, pivoted at an elevation high above the free surface in a water channel. In this case, with increasing flow velocities with both convex and concave arrangements, the frequency of cross-flow vibrations was initially about $0.2U/d$. But then from reduced velocities of about 5 it remained locked-on to the structural natural frequency, up to the highest reduced velocities tested, more than 18.

In most of the present experiments (as in all of those by Morooka and Tsukada (2013) and Fan et al. (2015)) the riser's profile was concave to the current. A convex shape occurred here only in those cases in which the upstream anchorage was at the surface, in the short transition between the lower part of the riser, lying on the floor of the tank under zero tension, and the upper part which hung in a straight line with the normal component of its weight balanced by drag.

The aim of the work described here was to contribute to an understanding of the motion of a highly flexible catenary riser in a steady current and to provide data for the validation of numerical models. We first describe the arrangements of the experiments, in which the response of the model riser, tensioned only by its own weight and the drag acting on it, was monitored by means of internal 3-axis accelerometers at 12 points over its length. The following section analyses the implications of contamination caused by the effect of gravity on the accelerometer signals. Subsequent sections deal with mean profiles of the riser in currents in both directions, and with the amplitudes and frequencies of the dynamic response in the cross-flow direction. It is found that typical dimensionless peak frequencies (having been normalised with respect to the diameter and a characteristic velocity) were in the range 0.11 to 0.13, in conditions in which the Strouhal number for vortex shedding from a stationary cylinder is close to 0.2.

2. EXPERIMENTAL ARRANGEMENTS

These experiments were carried out in the IFREMER recirculating water channel in Boulogne-sur-mer, France. This facility has an 18m long working section 4m wide, and it was operated with a water depth of 2m. Windows eight metres long provide an almost uninterrupted view of the flow from the side, over almost the full height of the channel. Measurements were carried out at flow speeds of between 0.2m/s and 1.4m/s, in which the incident turbulence level was 1.5%.

The design of the model riser was aimed at minimising bending stiffness and structural damping, rather than trying to reproduce the actual properties of a full scale riser. The model consisted of a 4mm diameter stainless steel wire rope, which passed concentrically through a large number of cylindrical nylon bobbins, each 30mm long and 54mm diameter. The bobbins were clamped on to the wire rope, with 10mm gaps between them, allowing the model riser to bend with radii of curvature of only a few diameters with very little resistance. A single length of medical silicone tubing, of 1mm wall thickness, passed over all the bobbins, providing the riser with an almost uniform outer diameter of 56mm. A short section is shown on the left in figure 1.

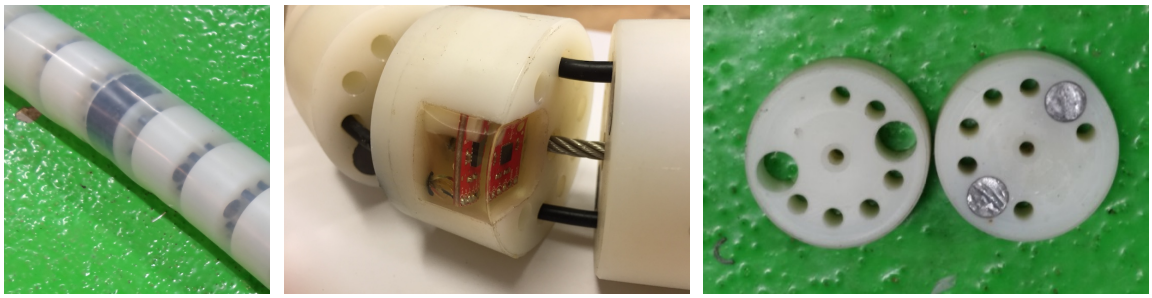

Figure 1. From left to right: a section of the riser showing bobbins (one of which, marked black, contains an accelerometer), and internal cables, all inside the silicone sheath; a bobbin with its built-in accelerometer in transparent potting compound; bobbins without and with lead inserts;

The overall length of the model riser between anchorages, where it was effectively pin-ended, was 5.36m. At intervals of 400mm, twelve of the nylon bobbins were instrumented with 3-axis Sparkfun ADXL335 analogue accelerometers, one of which can be seen in the middle photo in figure 1. Each

accelerometer was potted in a recess cut into its bobbin, preserving the bobbin's original shape. The density of both the nylon material of the bobbin and the potting compound was 1.15 g/cm^3 while that of an accelerometer (of mass 1g and volume 0.53 cm^3) was about 1.9 g/cm^3. The presence of an accelerometer in a bobbin therefore added about 0.4g to its original mass of 65.2g.

Electrical cables from the accelerometers passed freely through holes in the bobbins, to emerge, six at one end of the riser and six at the other. From there they were connected to signal conditioning amplifiers whose output, like that of tension load cells at each end of the riser, was sampled at 200Hz.

Key features of the model riser are set out in Table 1, where also some parameters are defined. From the initial conditions, an increase in the mass ratio m^* (the ratio of the mass of the riser, including internal water, to the mass of the water displaced by its cylindrical profile) was achieved by inserting a pair of lead plugs (of diameter 12.5mm and length 30mm) into longitudinal holes in the bobbins. This had the effect of raising the mass of each bobbin to 146.1g. Bobbins without, and with, lead plugs are shown on the right in figure 1. It was not possible to fit lead plugs into those bobbins that contained accelerometers, and consequently those 12 that were instrumented, out of a total of 119, were lighter than the others by 55% in these tests. It is not clear how this local reduction in mass affected the response, but it is worth noting that the vibration wavelength was typically about 1m, covering around 25 bobbins.

The internal damping of the model riser was estimated by hanging it vertically between fixed points and vibrating it manually over a range of frequencies to excite different structural modes, which were then allowed to decay freely. The bending stiffness and the axial stiffness listed in Table 1 were estimated using the mechanical properties of the elements of the model.

The accelerometers were calibrated in-situ. One of the axes of each accelerometer was aligned with the axis of the riser, and it could be calibrated by raising the riser, or part of it, into the vertical, first one way and then the other. The other two accelerometer axes, aligned along orthogonal normal to the riser's axis were calibrated by slowly rolling the assembled riser on the floor of the laboratory. In each case the output range corresponded to 2g, and the mid-range point to zero.

The measurements discussed in this paper come from four series of tests, with the riser on the central longitudinal axis of the channel, with two mass ratios, and two flow directions. Figure 2 shows the riser installed in the tank.

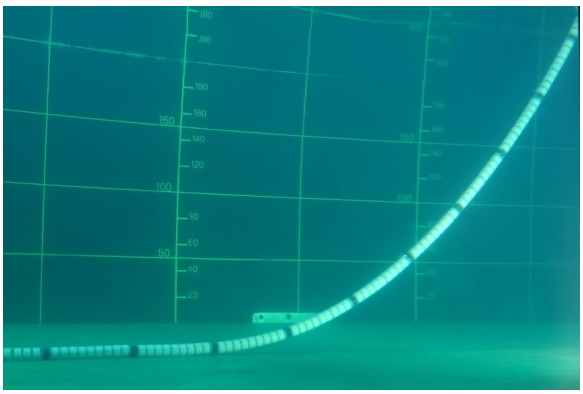

Figure 2. The model riser in a slow current (flowing from left to right). The bobbins containing accelerometers are black. In this case the first 5 of them were on the floor of the tank.

	Series 1	Series 2
Diameter *d*	56mm	
Length between pin ends	5.36m	
Estimated bending stiffness EI	1.3Nm^2	
Estimated axial stiffness EA	790kN	
Implied Young's modulus	3.2 x 10^{8}N/m^2	
Structural damping in air	About 3% of critical	
Submerged weight *W*	2.9N/m	20.9N/m
Mass ratio *m**	1.12	1.84
Water depth	2.0m	
Lower anchorage	On the tank floor	
Upper anchorage elevation	200mm above the water surface	
Horizontal distance between pin ends	4.30m	
Flow speeds *U*	0 to $\pm$ 1.4m/s	
Maximum Reynolds number	70,000	

Table 1. Details of the model riser

3. SIGNAL PROCESSING

This section outlines the method by which the measured accelerations were used to estimate the mean profile of the riser, and to identify features of its dynamic displacements. Accelerometers of the kind used here record the effects of gravity and so detect changes in their inclination from the vertical as well as linear acceleration. For this reason, when they are used for the purpose of measuring displacements, the results may be (and in this case, were) contaminated by gravity. In general, with a single 3-axis accelerometer it is not possible to separate these gravitational contributions from the linear accelerations of interest.

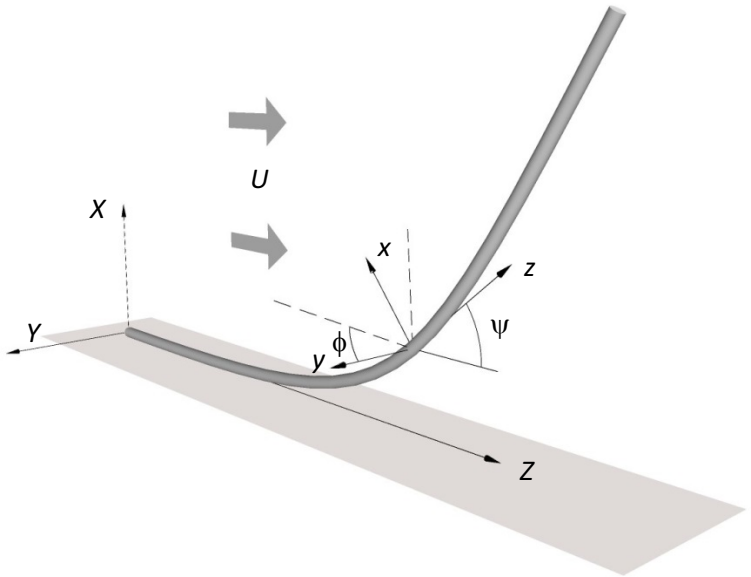

Figure 3. Definition sketch showing global (*X*, *Y*, *Z*) and local (*x*, *y*, *z*) coordinates; ψ is the local inclination of the riser to the horizontal. One accelerometer axis is aligned with the *z*-axis on the local tangent, the other two with the broken lines in the (*x*, *y*) plane, the first of which makes an angle ϕ with the *y*-axis.

The sketch in figure 3 defines global coordinates (*X*, *Y*, *Z*), with *Z* measured horizontally from the upstream end of the riser, and *X* measured vertically upwards. At any point along it, a local system (*x*, *y*, *z*) is defined with *z* measured in the tangential direction and (*x*, *z*) in the vertical plane. The local inclination of the riser to the horizontal is ψ . The two accelerometer axes in the normal (*x*, *y*) plane at each instrumented bobbin are aligned at some initially unknown orientations ϕ and $\phi+\pi/2$ to the *y* axis. The third accelerometer axis lies along the tangent, coinciding with the *z* axis. Acceleration signals recorded on these three axes are denoted $a_1(t)$, $a_2(t)$ and $a_z(t)$,respectively. As described below, frequencies of accelerations in the local *x* (in-plane) and *y* (cross-flow) directions, as well as the mean profile of the riser in the (*X*, *Z*) plane, can be estimated from these records.

If the riser were stationary, the direction cosine of the local tangential (*z*) axis, with reference to the global vertical (*X*) axis, would be $\ell_z = \sin\psi$, and an accelerometer on the *z* axis would register $g\ell_z$. The corresponding direction cosine of an accelerometer axis that is orientated at some angle ϕ from the local *y* axis in the normal plane, would be $\ell_\phi = \cos\psi\sin\phi$. To determine the gravitational contamination in measurements of acceleration on each of these accelerometer axes when the riser was vibrating, it is helpful to calculate the resulting changes in ℓ_z and ℓ_ϕ .

Consider first the effect of displacements in the (*X*, *Z*) plane of the form

$$x = A\sin ks\cos\omega t,\ y = 0\ , \tag{1}$$

where *s* is measured along the riser and the wavelength of the disturbance is $2\pi/k$. Then these two direction cosines become

$$\ell_z = \sin\left(\psi + \arctan\left(kA\cos ks\cos\omega t\right)\right) \text{ and } \ell_\phi = \cos\left(\psi + \arctan\left(kA\cos ks\cos\omega t\right)\right)\sin\phi\ . \tag{2}$$

Typical wavelengths of the vortex-induced vibrations of the riser were in the region of one metre, and maximum displacements were around one diameter, corresponding to $kA \approx 0.3$. It therefore seems reasonable to express equations (2) in the form of power series in kA . Multiplying by g, the gravitational component $a'_{z,\mathrm{IL}}(t)$ in the measured axial acceleration $a_z(t)$ due to vibrations of the form of equation (1) is then

$$a'_{z,\mathrm{IL}}(t) = g\left[\left(1-\frac{k^2A^2\cos^2 ks}{4}\right)\sin\psi + kA\cos ks\cos\psi\cos\omega t - k^2A^2\frac{\cos^2 ks}{4}\sin\psi\cos 2\omega t + O(k^3A^3)\right], \tag{3}$$

and the corresponding gravitational component in measurements of acceleration on an axis in the normal (x, y) plane is

$$a'_{1,\mathrm{IL}}(t) = g\sin\phi\left[\left(1-\frac{k^2A^2\cos^2 ks}{4}\right)\cos\psi - kA\cos ks\sin\psi\cos\omega t - k^2A^2\frac{\cos^2 ks}{4}\cos\psi\cos 2\omega t + O(k^3A^3)\right]. \tag{4}$$

The term in k^2A^2 in the time-independent part of (3) represents the component of the mean of the acceleration signal in the tangential direction that is caused by the vibrations. Therefore a first approximation to the mean inclination of the riser at the location of an accelerometer could in principle be obtained from

$$\bar{\psi}_1 = \arcsin \frac{\overline{a_z(t)}}{g\left(1 - \dfrac{k^2A^2\cos^2 ks}{4}\right)}, \tag{5}$$

where $\overline{a_z(t)}$ is the time average of the accelerometer signal $a_z(t)$. But in practice, for the purposes of computing the riser's mean inclination at each accelerometer, the unknown second part of the denominator in (5) was neglected, giving an estimate: $\bar{\psi} = \arcsin\left(\overline{a_z(t)}/g\right)$. With *kA* = 0.3 this simplification would lead to errors in $\bar{\psi}$ increasing from zero where the riser was horizontal, to a maximum (at nodes) of 4° at $\bar{\psi}_1 = 70^o$, and 12° at $\bar{\psi}_1 = 90^o$.

From a set of mean inclinations obtained in this way, a first estimate of the riser's mean profile from end to end in the (*X*, *Y*) plane could be obtained by a numerical shooting method starting from the anchorage on the tank floor. In an iterative process successive corrections were then applied to each of the approximate mean inclinations to minimise the distance between the computed end of the riser and the known location of the upper anchorage point. Good qualitative comparisons between profiles computed in this way from accelerometer records and photographs are shown below.

The effects of gravity on accelerometer measurements of in-plane vibrations can be seen in the second term in square brackets in equations (3) and (4). In relation to the amplitude of actual linear accelerations $A\omega^2$, the amplitude of the gravitational effects due to vibrations of the form of equation (1) are $gk\cos\psi/\omega^2$ and $gk\sin\phi\sin\psi/\omega^2$ in the in-plane and cross-flow directions respectively. With a wavelength of 1m ($k = 2\pi \text{m}^{-1}$) and a frequency of 2Hz these ratios can amount to as much as 40%. Smaller contributions arise at twice the fundamental frequency.

Similarly, in the case of vibrations purely in the cross-flow (*y*, *z*) plane with displacements of the form

$$x = 0,\ y = A\sin ks\cos\omega t\ , \tag{6}$$

estimates of the gravitational content of accelerometer measurements in the *z* and *y* directions are

$$a'_{z,\text{CF}}(t) - g\left[\left(1 - \frac{k^2A^2\cos^2 ks}{4}\right)\sin\psi - k^2A^2\frac{\cos^2 ks}{4}\sin\psi\cos 2\omega t + O\left(k^4A^4\right)\right] \tag{7}$$

and

$$a'_{1,\text{CF}}(t) = -gkA\sin\phi\ \sin\psi\cos ks\ \cos\omega t + O\left(k^3A^3\right) \tag{8}$$

respectively, indicating contamination of similar magnitudes.

In the light of these results it seems unlikely that time series of in-plane or cross-flow displacements can be obtained reliably from acceleration measurements alone, except where the riser makes a small angle with the horizontal, say $\sin\psi < 0.1$ or $\psi < 5^\circ$. In other cases, gravitational effects would have to be removed from the signals, for example by incorporating 3-axis gyros, and performing the double integration needed to obtain displacements. Nevertheless, it is also evident from the analysis above that dynamic gravitational contributions, predominantly proportional to the vibration amplitude, are substantially at the same frequency as the vibration of the riser. The amplitude of those gravitational components that appear at twice the dominant frequency represent increments of only a few percent.

The application of these conclusions in the present case is based on the assumption that the model riser did not undergo any torsional displacements about its own axis. It was very flexible in all degrees of freedom, and digital analysis of video records revealed rotations with standard deviations of up to about 5°, synchronised with the cross-flow vibration. The consequence of this was some cross-talk between measurements of cross-flow and in-line accelerations, but no change in the perceived dominant frequencies observed in either direction.

The mean orientations of the two accelerometer axes that were perpendicular to the axis of the riser could be estimated from $\bar{\phi} = \arctan\left[\overline{a_2(t)} / \overline{a_1(t)}\right]$. Acceleration records transformed to the *x* and *y* axes are referred to as the normal in-plane component and the cross-flow component respectively. (The former is not the same as what is usually referred to as the in-line component since it is not in the direction of the incident flow.)

In a large number of tests the motion of the riser was also recorded with two underwater video cameras generally looking vertically downwards to record simultaneously the motion of up to three of the instrumented bobbins each. Image processing provided time series of displacements in the cross-flow (*y*) and horizontal in-plane (*Z*) directions, of much better quality than any that could be derived from accelerometer recordings.

Though time series of the riser's displacements could not be inferred from the acceleration measurements with any confidence, it seems reasonable nevertheless to assume that the shape of their spectra would be very similar to those obtained by double integration of the acceleration signals. From equations (3, 4, 7) it can be seen that double frequency components introduced by the effect of gravity are proportional to gk^2A^2; in the present conditions this would have a small effect on computed spectra, and in any case would not significantly shift the peak frequency. As a check on this, spectra of the doubly-integrated cross-flow accelerometer measurements are plotted in the lower row in figure 4 for three flow velocities with $m^* = 1.84$. Above them are shown spectra derived from video records of displacements for the same cases. As anticipated the variances of the signals do not match very well, but corresponding peak frequencies are almost identical. With this in mind it seems reasonable to compute peak frequencies from either source of data: accelerometer measurements or video recordings.

The configuration shown in figure 3, with the upstream anchorage on the tank floor and the downstream one near the surface, defines what is referred to here as a positive current; $U > 0$. This is how the arrangement was viewed in the laboratory, where the effect of flow in the opposite direction could be achieved only by reversing the elevations of the upstream and downstream anchorages. However, for present purposes, all images and plots for negative flow cases are shown mirrored right to left, as if it had been possible to reverse the flow in the tank.

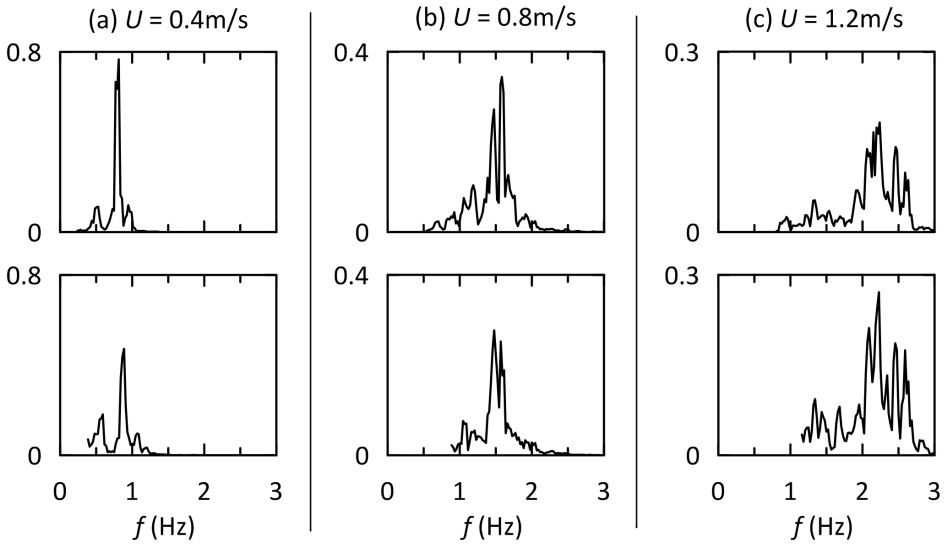

Figure 4. Spectra of cross-flow displacements derived from video records (above), and from doubly-integrated accelerations (below) at three flow speeds; m^* = 1.84. The doubly-integrated plots have been truncated to remove their explosive behaviour at low frequencies. These records are from a point on the riser identified by a cross on the profiles shown on the right in figure 6.

4. RESULTS AND DISCUSSION

4.1 Positive currents

For positive currents, figure 5 shows mean profiles of the riser computed from axial accelerometer records, with inclined arrows indicating the direction of changes that result from increasing the flow speed. Not surprisingly this effect is greater for the lighter riser (on the left) than the heavier one, resulting in larger upstream displacements of the touch-down point.

Figure 6 shows representative time series of displacements in the cross-flow (y) and in-plane horizontal (Z) directions for the riser with m^* = 1.84 at three flow speeds. Features that are familiar from the observed response of long vertical tensioned risers and flexible cylinders include peak cross-flow displacements that rarely exceed one diameter, in-line displacements containing higher frequency components of a smaller amplitude, and frequencies increasing with the flow speed. But a notable difference is that the motion here is generally more irregular and subject to modulations in frequency.

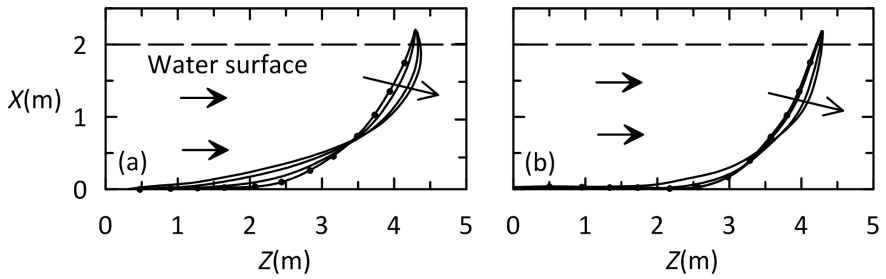

Figure 5. Mean profiles computed from accelerometer records for current speeds from 0 to +1.4m/s. On the left, m^*=1.12; on the right, m^*=1.84. Symbols indicate the positions of the accelerometers and inclined arrows indicate the effect of increasing current speeds.

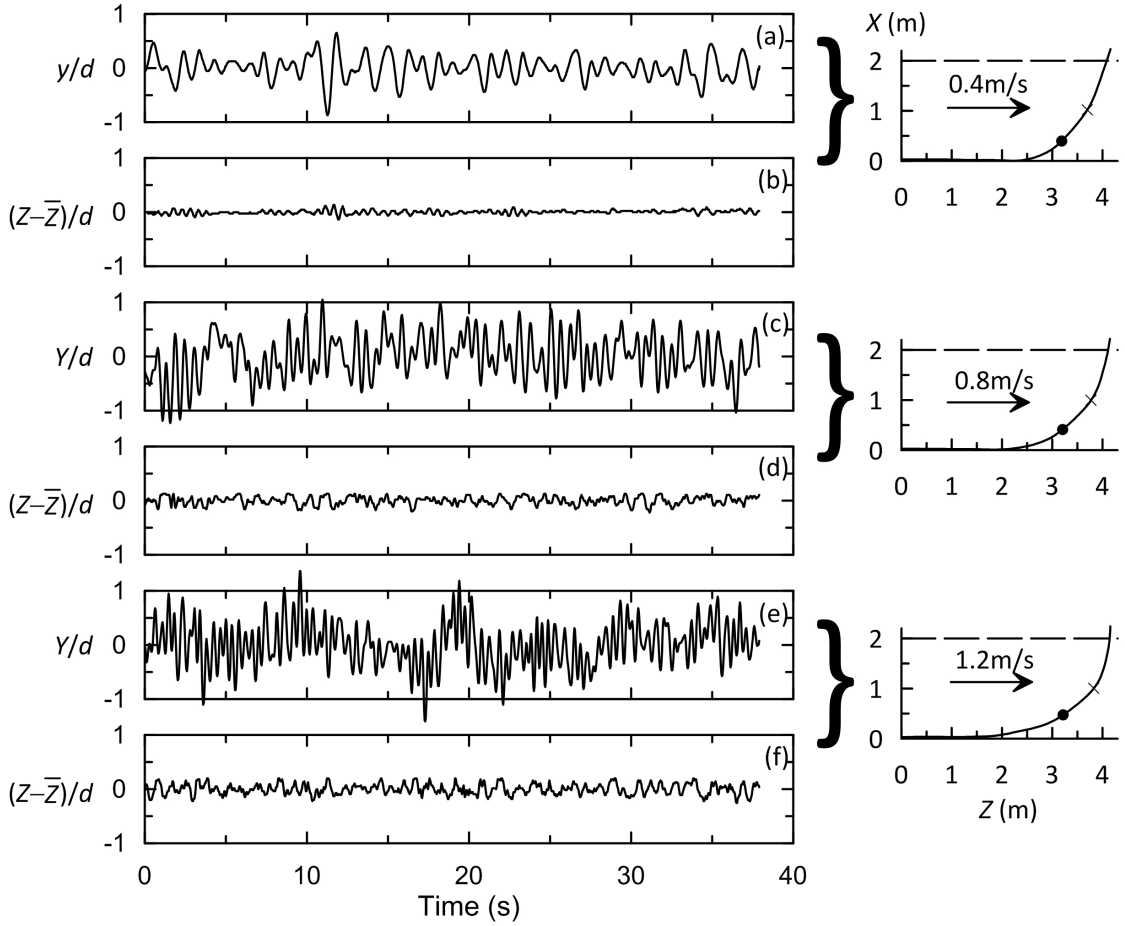

Figure 6. Time series of displacements of the riser in the crossflow (y) and in-plane horizontal (Z) directions at three positive current speeds: (a, b) 0.4m/s; (c, d) 0.8m/s; (e, f) 1.2m/s. These results are for the heavier riser (m^* = 1.84), at the points along the riser identified by solid symbols in the respective mean profiles shown on the right.

Spectra of accelerations measured at the same point as the time series in figure 6, and at the same three flow speeds, are shown in the top two rows of figure 7. Dotted lines refer to the lighter riser, continuous lines to the heavier one. Those for the cross-flow direction (in the top row) have clearly-defined peak frequencies which increase with the current. In the in-plane direction (second row) the peaks are not all so distinct, but are centred around twice the corresponding cross-flow frequency as expected.

The third row of plots show how these peak cross-flow frequencies vary over that section of the riser that is off the floor, seen in the mean profiles plotted below. In each case the frequencies are substantially uniform along the riser at each flow speed, except for the region near the top where there is a small increase, possibly associated with aeration of the wake and a reduction in added mass due to the proximity of the free surface. Consequently, dimensionless frequencies $fd/U\sin\psi$ based on local normal velocities $U\sin\psi$, are far from uniform, varying from 0.11 near the top of the riser to more than 0.3 below, as shown in figure 8.

Plotting the same cross-flow frequencies against the current speed *U* (which is within 3% of the normal velocity at the top of the riser in all cases) on the other hand, reveals much greater uniformity over most of the range, as shown in figure 9, where most points lie close to $f = 0.11U/d$. However at locations in the bottom half of the riser, some peaks appear at still lower frequencies (figure 9(b)). Some of these, for the heavier riser are at about one half of the dominant peak frequency.

It seems reasonable to infer that the response of the lower part of the riser, where it is more curved, inclined at a shallower angle to the flow (factors which tend to mitigate against regular VIV), and under lower tension, is largely controlled by the vortex-induced vibrations in the region near the top. It is not clear however why the dominant frequency should be so much lower than that which can be expected in the case of a vibrating vertical tension riser or cylinder in a cross flow.

In comparable experiments Morooka and Tsukada (2013) compared measured peak frequencies with estimated modal frequencies of their model riser. This approach could provide some insight into the unexpected frequencies observed in the present case, but bearing in mind that structural modal frequencies are functions of the profile, the unknown non-uniform tension, and the effective length to the touch-down point, all of which depend on the vibration-enhanced drag, it was not clear that this exercise could be carried out with much confidence or precision, and was not attempted here.

Dominant frequencies over most of the length of the riser, plotted in figure 9, are almost the same for both riser weights, increasing linearly with the flow speed. That they do so despite large changes in the tension (shown in figure 12) and profile that would give rise to more complicated shifts in structural modal frequencies, suggests that these vibrations were not controlled by lock-in.

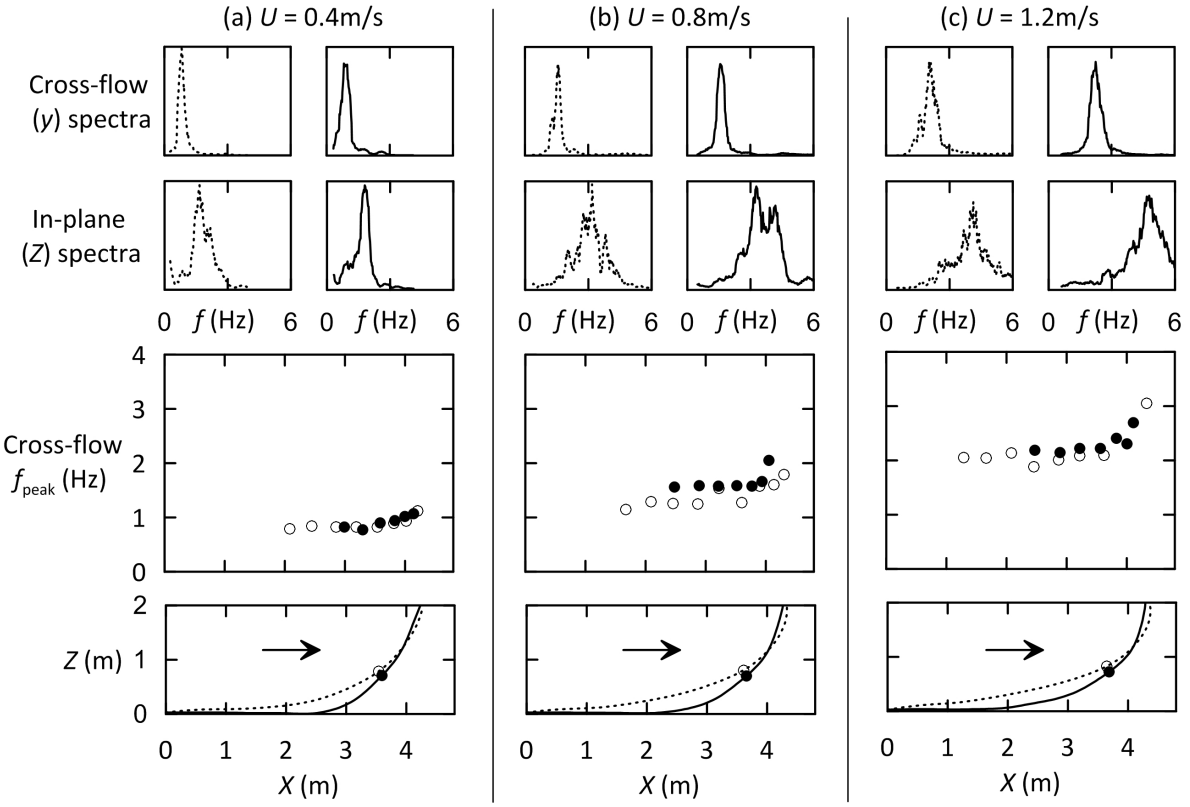

Figure 7. Spectra and peak frequencies in positive currents. The top two rows show spectra of cross-flow and in-plane accelerations at points on the mean profiles identified in the bottom row. The third row shows spectral peak frequencies in cross-flow accelerations, plotted as functions of horizontal distance along the riser, at (a) 0.4m/s; (b) 0.8m/s; (c) 1.2m/s. Open symbols and broken lines, m^* = 1.12; solid symbols and continuous lines, m^* = 1.84.

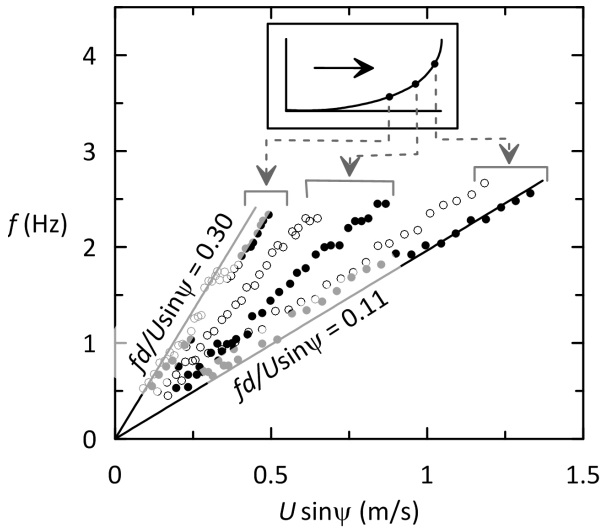

Figure 8. Cross-flow peak frequencies at three points along the riser as functions of the local normal incident velocity; open symbols, m^* = 1.12: solid symbols, m^* = 1.84.

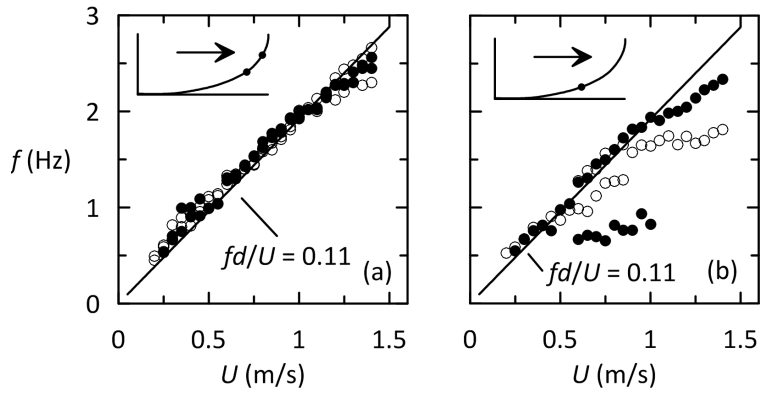

Figure 9. Spectral peak frequencies in cross-flow accelerations at selected points on the riser, plotted as functions of flow speed. Locations of the accelerometers are shown in the inset diagrams; open symbols, m^* = 1.12: solid symbols, m^* = 1.84.

.

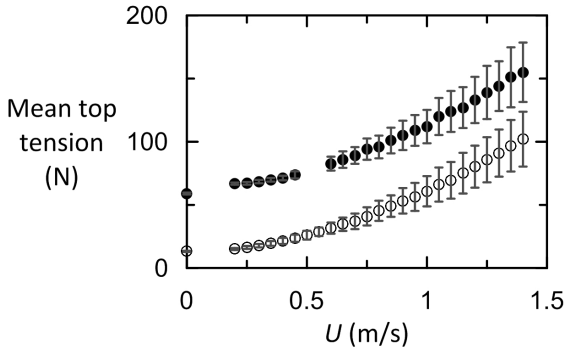

Figure 10. Mean top tensions in positive currents; open symbols, m^* = 1.12: solid symbols, m^* = 1.84. Error bars extend up and down by one standard deviation.

4.2 Negative currents

In negative currents, flowing in the $-Z$ direction in the sketch in figure 3, the riser behaved quite differently. Also there were important differences between its responses at the two mass ratios. Photographs in figure 11 show the mean shapes taken up by the lighter model riser on the left and the heavier one on the right, in a current U (now measured in the opposite direction) of 0.6m/s. This was sufficient to lift the lighter riser over its entire length, while at the same speed almost half of the heavier one remained on the tank floor.

Corresponding profiles computed from axial accelerometer signals, also shown in figure 11, have similar shapes. At most speeds, at least some part of the riser adopted an almost straight line mean profile, in which the normal component of the drag is balanced by the normal component of the submerged weight, without any contribution from the tension. As long as the lower part of the riser rested freely on the tank floor so that the tension there approached zero, this situation has much in common with that of a free-hanging riser (Wang et al., 2017). This was the state of affairs for U <

0.5m/s for m^* = 1.12, and U < 1.0m/s for m^* = 1.84. At higher speeds in both cases the riser was held down to the tank floor at the bottom anchorage, causing the tension to increase throughout. Also, at low speeds (U < 0.2m/s for m^* = 1.12, and U < 0.5m/s for m^* = 1.84) the profiles remained curved from top to bottom because the drag had little effect on the initial catenary. Both features can be seen in the profiles in figure 11.

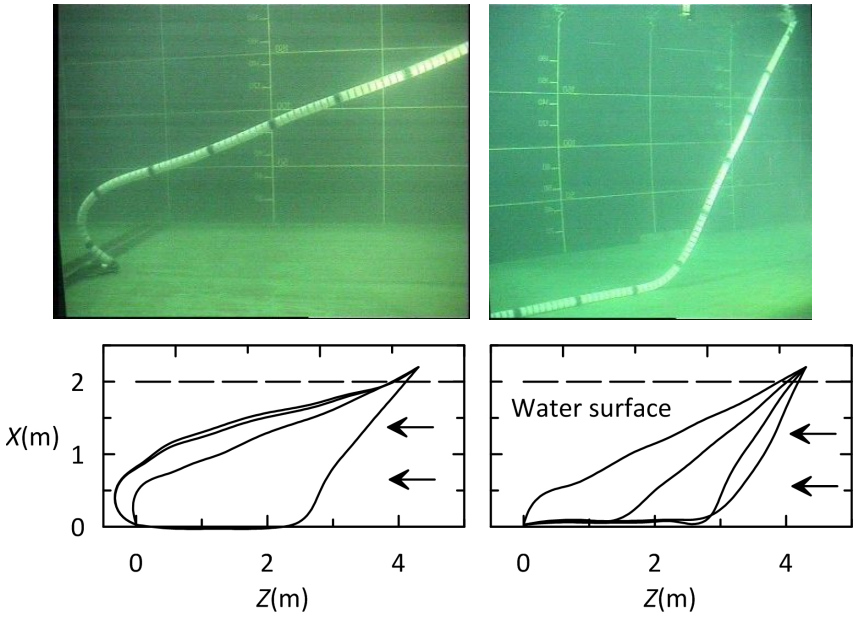

Figure 11. The risers of both mass ratios in a negative current: in the photographs, U = 0.6m/s with m^*=1.12 on the left and m^*=1.84 on the right. Plots below show mean profiles computed from accelerometer records for U = 0.3m/s, 0.6m/s, 0.9m/s, 1.2m/s.

The independence principle provides a basis for estimating the inclination of the straight line profile where it existed. Equating the drag, estimated from the normal velocity, to the normal component of the weight, leads to

$$\sin\psi = \frac{1}{\sqrt{\sqrt{\frac{F^2}{W^2}+\frac{1}{4}}+\frac{1}{2}}}, \text{ where } F = C_d \tfrac{1}{2}\rho U^2 d\,. \tag{9}$$

For a given drag coefficient this prediction can be compared with the measured inclinations computed from the axial accelerometer signals. These are plotted for both riser weights as functions of flow speed in figure 12(a). Inclinations computed from equation (9) for $C_d = 2.0$ and 2.8, shown as broken lines, bracket most of the measurements. Drag coefficients of such magnitudes are not unexpected; according to the formula proposed by Chaplin et al. (2005) based on measurements of drag on a long vertical riser, an increase of 180% in C_d could be caused by cross-flow vibrations with a standard deviation of less than 60% of a diameter.

In figure 12(b) normal components of velocity calculated from equation (9) for the same two drag coefficients again bracket those based on the measurements. It is interesting to note that for m^* =

1.12 throughout, and for m* = 1.84 when U was greater than about 0.5m/s, the normal velocity $U\sin\psi$ was approximately constant. Indeed, it is a consequence of equation (9) is that as U increases, the riser would align itself so that the normal component of velocity approaches a constant value, namely

$$U\sin\psi \to \sqrt{\frac{2W}{C_d \rho d}}\,. \tag{10}$$

This is indicated by arrows on the right hand axis of figure 12(b) for the same two drag coefficients.

Another consequence of equation (9) is that if the riser adopted a straight line profile over its entire length the top tension would be Wh in all cases, where h is the water depth. Figure 13 shows that this is a good approximation to measured top tensions in the ranges of current speeds mentioned above, namely 0.2m/s < U < 0.5m/s for m* = 1.12, and 0.5m/s < U < 1.0m/s for m* = 1.84.

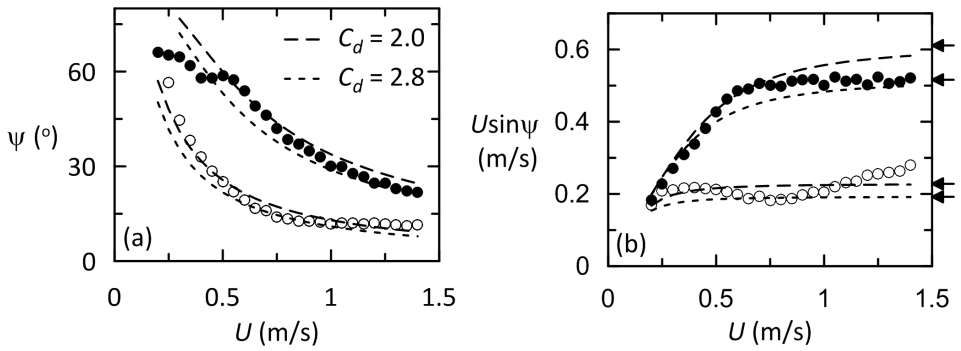

Figure 12. (a) Mean inclinations of the straight part of the model riser as functions of flow speed. Broken lines are calculated from equation (9) for the drag coefficients indicated. (b) Corresponding normal components of velocity; arrows on the right hand axis indicate limiting values of $U\sin\psi$ as U tends to infinity; open symbols, m* = 1.12: solid symbols, m* = 1.84.

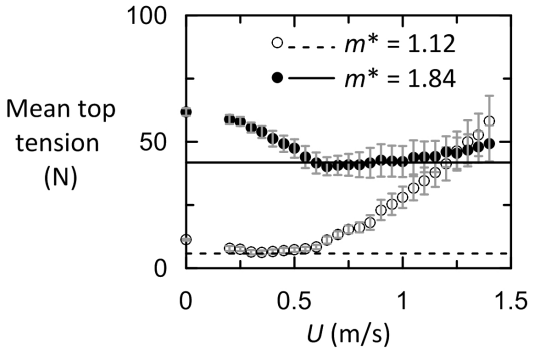

Figure 13. Mean top tensions as functions of current speed. Lines indicate the product of the total submerged weight and the water depth. Error bars extend up and down by one standard deviation.

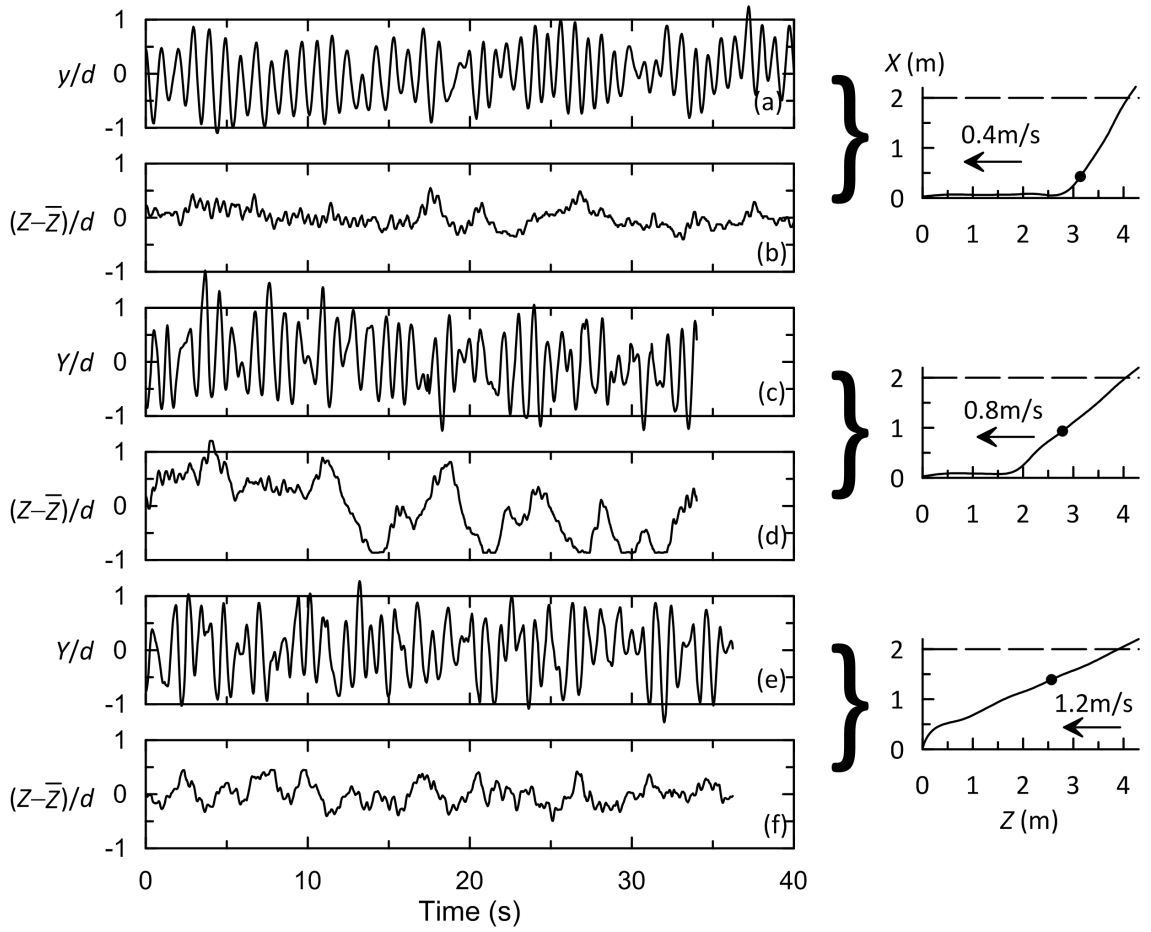

Figure 14. Time series of displacements of the riser in the crossflow (*y*) and in-plane horizontal (*Z*) directions at three negative current speeds: (a, b) 0.4m/s; (c, d) 0.8m/s; (e, f) 1.2m/s. These results are for the heavier riser (m^* = 1.84), at the points along the riser identified by solid symbols in the respective mean profiles shown on the right.

It follows from the discussion above that if the independence principle applied in these conditions, the vortex shedding frequency, like the normal component of velocity, might be expected to be independent of the current speed, in the absence of lock-in. Time series of cross-flow displacements plotted in figure 14 appear to provide some support for this idea. Unlike the case of a positive current (figure 6), the dominant frequency of response in the cross-flow direction in negative currents can be seen to be roughly the same at all three speeds shown.

Figure 15(a) shows that for both mass ratios there are regions (0.4m/s < *U* < 0.8m/s for m^* = 1.12, and 1.0m/s < *U* < 1.4m/s for m^* = 1.84) in which cross-flow spectral peak frequencies (measured at points at around mid-depth) are indeed largely independent of the current speed. These frequencies are closely represented by $f = 0.13U\sin\psi / d$, based on the normal velocity (figure 15(b)) It is the nature of the response that in any given conditions there were multiple peaks in the spectra, and several of these are included in figure 15. As shown here, peak frequencies found in the response of the lighter riser increased rapidly with current speeds above 0.8m/s, probably because of the

influence of the increasing tension (see figure 13) on structural modal frequencies. Already by 0.5m/s the touch-down point had advanced so far downstream that the riser had begun to be held down with increasing force at the anchorage. It therefore seems likely that in these conditions (m^* = 1.12, U > 0.8m/s) the response was locked in to a structural frequency.

Conversely, with the heavier riser, most of the downstream displacement of the touch-down point took place from 0.6m/s to 1.0m/s, with little change in the tension. Modal frequencies would therefore have been decreasing. So it seems reasonable to conclude that the downwards trend in peak frequencies shown in figure 15(a) in the middle range of current speeds can again be caused by lock-in. As shown in figure 15(b) all other points again lie close to the line S_N = 0.13.

As before, peak cross-flow frequencies, plotted in the third row of figure 16 for both mass ratios, are almost uniform over that part of the riser that is away from the floor. Spectra shown above reveal the increasingly complex distributions as the current speed was increased.

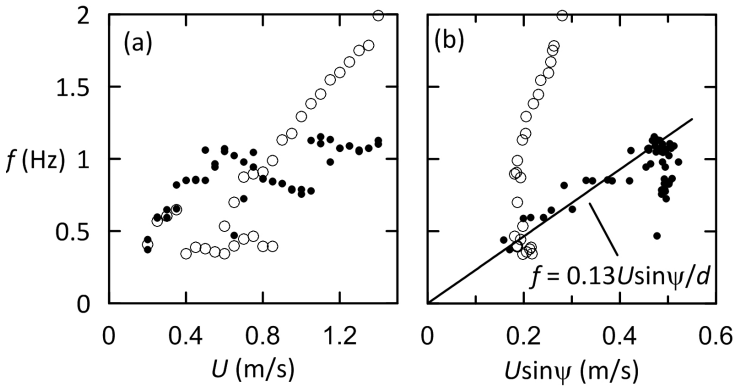

Figure 15. Dominant frequencies of cross-flow vibrations as functions of (a) current speed, (b) normal incident velocity in negative currents; open symbols, m^* = 1.12: solid symbols, m^* = 1.84.

5. CONCLUSIONS

Laboratory measurements of vortex-induced vibrations of a flexible catenary model riser with very low bending stiffness, high curvature, and tensioned only by its own weight and drag, were made in steady currents at Reynolds numbers up to 70,000. The length to diameter ratio was 95, and tests were carried out with two mass ratios, 1.12 and 1.84. At low current speeds the bottom end of the riser lay on the tank floor, while at the top it passed almost vertically through the water surface, 2m above, and 4.3m up- or downstream. Measurements of the inclination of the riser to the vertical, and of frequencies of response, were inferred from signals from twelve 3-axis internal accelerometers distributed along the riser, after due attention had been given to the problem of gravitational contamination. Measurements of displacements were obtained by processing videos recorded by underwater cameras.

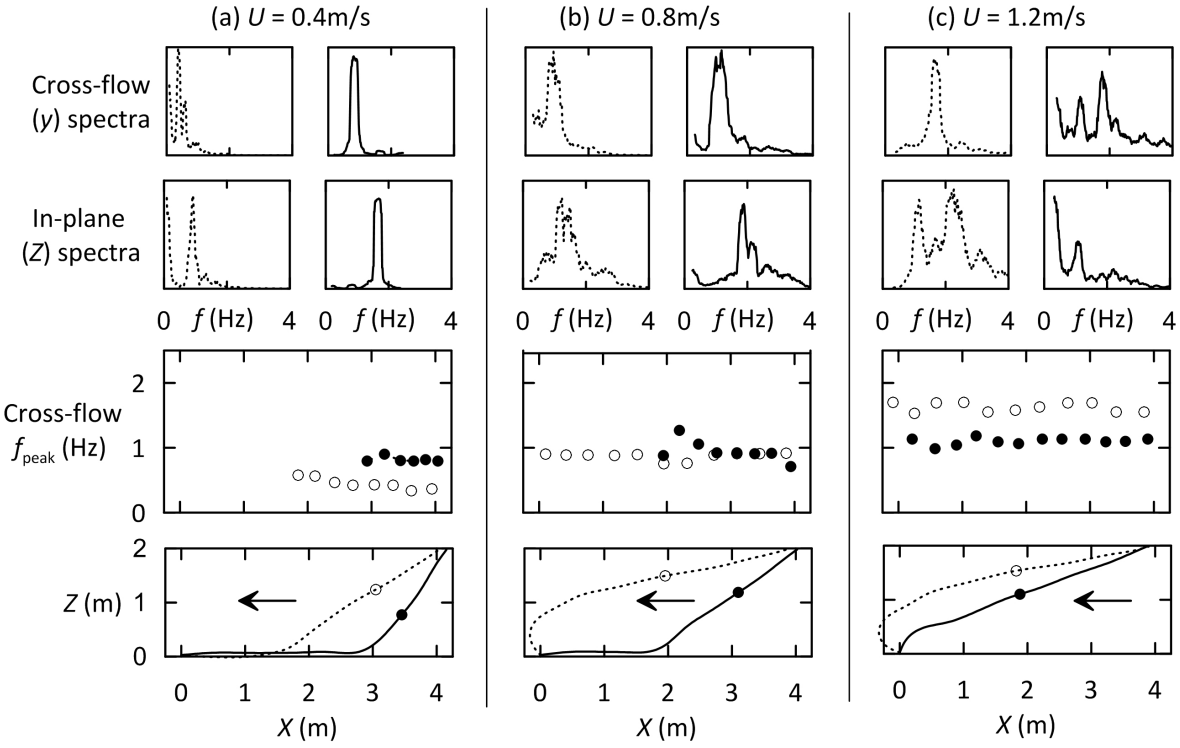

Figure 16. Spectra and peak frequencies in negative currents. The top two rows show spectra of cross-flow and in-plane accelerations at points on the mean profiles identified in the bottom row. The third row shows spectral peak frequencies in cross-flow accelerations, plotted as functions of horizontal distance along the riser, at (a) 0.4m/s; (b) 0.8m/s; (c) 1.2m/s. Open symbols and broken lines, m^* = 1.12; solid symbols and continuous lines, m^* = 1.84.

The results reveal some complex behaviour that is not familiar from previous studies of the vibrations of straight tensioned vertical risers and spring-mounted cylinders. In general, acceleration and displacement spectra were more broad-banded, and often contained multiple peaks, sometimes closely-spaced. Peak frequencies, normalised with respect to a characteristic velocity and the diameter, were often well below the familiar range of 0.16 to 0.2, though amplitudes of motion were mostly in the range of one diameter.

The model riser behaved quite differently in positive and negative currents, i.e. those in which the upstream end was on the tank floor and the downstream end was at the surface, and vice-versa. In positive currents the profile of the riser changed little over the range of flow speeds from 0.2m/s to 1.4m/s, as the upper part was displaced downstream and more of the lower part (depending on the riser's submerged weight) was lifted off the tank floor, displacing the touch-down point upstream. Peak frequencies of cross-flow response were predominantly uniform over the whole length of the riser (despite large changes in its inclination) and generally increased linearly with the flow speed. The normalised frequency, based on the peak cross-flow frequency and the current speed (the same as the normal incident velocity at the top of the riser to within a few percent) was 0.11.

In a negative current the riser adopted a straight line profile over most of the distance between the water surface and the touch-down point, at an inclination at which the (upwards) normal component of drag balanced the normal component of its weight. On the basis of the independence

principle the drag coefficient deduced from the angle that the riser made with the horizontal was estimated at between 2.0 and 2.8, in line with earlier measurements of vibration-enhanced drag. Another consequence of the straight-line profile observed in negative currents is that the normal component of velocity, being uniform over a substantial proportion of the length of the riser, can be expected to give rise to vortex shedding at a uniform frequency independent of the current speed. The measurements provided some support for this conclusion, and were consistent with a normalised frequency of 0.13, based in this case on the normal component of velocity.

Experimentally as well as computationally, modelling and understanding the dynamics of a very flexible untensioned catenary riser or marine cable subject to vortex-induced excitation is much more challenging than studying the case of a vertical tensioned riser or elastically-mounted cylinder. Much more work following both approaches needs to be carried out in order to develop a better understanding of responses and loadings of related offshore systems.

ACKNOWLEDGEMENTS

This work was funded by EPSRC under grant EP/K034251. The authors thank Dr Toru Tsuzaki and the technical staff at the IFREMER re-circulating water channel for their expert assistance throughout the tests.

REFERENCES

Assi, G.R.S., Srinil, N., Freire, C.M., Korkischko, I., 2014. Experimental investigation of the flow-induced vibration of a curved cylinder in convex and concave configurations. Journal of Fluids and Structures 44, 52-66.

Chaplin, J.R., Bearman, P.W., Huarte, F.J.H., Pattenden, R.J., 2005. Laboratory measurements of vortex-induced vibrations of a vertical tension riser in a stepped current. Journal of Fluids and Structures 21, 3-24.

Chatjigeorgiou, I.K., Damy, G., LeBoulluec, M., 2008. Numerical and experimental investigation of the dynamics of catenary risers and the riser-induced-damping phenomenon, ASME 27th International Conference on Offshore Mechanics and Arctic Engineering. ASME, Estoril.

Fan, Y.-t., Mao, H.-y., Guo, H.-y., Liu, Q.-h., Li, X.-m., 2015. Experimental investigation on vortex-induced vibration of steel catenary riser. China Ocean Engineering 29, 691-704.

Gu, J.J., Vitola, M., Coelho, J., Pinto, W., Duan, M.L., Levi, C., 2013. An experimental investigation by towing tank on VIV of a long flexible cylinder for deepwater riser application. Journal of Marine Science and Technology 18, 358-369.

Huera-Huarte, F.J., Bearman, P.W., 2009. Wake structures and vortex-induced vibrations of a long flexible cylinder-Part 1: Dynamic response. Journal of Fluids and Structures 25, 969-990.

Jain, A., Modarres-Sadeghi, Y., 2013. Vortex-induced vibrations of a flexibly-mounted inclined cylinder. Journal of Fluids and Structures 43, 28-40.

Kim, W.J., Newlin, J.A., Haws, J.H., 2006. Experimental and analytical investigation of soil/SCR interaction under VIV, 16th International Offshore and Polar Engineering Conference (ISOPE 2006), San Francisco, CA, pp. 68-75.

King, R., 1977. Vortex excited oscillations of yawed circular-cylinders. J. Fluids Eng.-Trans. ASME 99, 495-502.

Miliou, A., De Vecchi, A., Sherwin, S.J., Graham, J.M.R., 2007. Wake dynamics of external flow past a curved circular cylinder with the free stream aligned with the plane of curvature. Journal of Fluid Mechanics 592, 89-115.

Morooka, C.K., Tsukada, R.I., 2013. Experiments with a steel catenary riser model in a towing tank. Applied Ocean Research 43, 244-255.
Pereira, F.R., Goncalves, R.T., Pesce, C.P., Fujarra, A.L.C., Franzini, G.R., Mendes, P., Asme, 2013. A model scale experimental investigation on vortex-self induced vibrations (VSIV) of catenary risers. Proceedings of the Asme 32nd International Conference on Ocean, Offshore and Arctic Engineering - 2013 - Vol 7.
Ramberg, S.E., 1983. The effects of yaw and finite length upon the vortex wakes of stationary and vibrating circular-cylinders. Journal of Fluid Mechanics 128, 81-107.
Trim, A.D., Braaten, H., Lie, H., Tognarelli, M.A., 2005. Experimental investigation of vortex-induced vibration of long marine risers. Journal of Fluids and Structures 21, 335-361.
Wang, J.A., Fu, S.X., Wang, J.S., Li, H.J., Ong, M.C., 2017. Experimental Investigation on Vortex-Induced Vibration of a Free-Hanging Riser Under Vessel Motion and Uniform Current. J. Offshore Mech. Arct. Eng. Trans. ASME 139.
Wang, J.G., Fu, S.X., Baarholm, R., Wu, J., Larsen, C.M., 2015a. Out-of-plane vortex-induced vibration of a steel catenary riser caused by vessel motions. Ocean Eng. 109, 389-400.
Wang, K.P., Tang, W.Y., Xue, H.X., 2015b. Time domain approach for coupled cross-flow and in-line VIV induced fatigue damage of steel catenary riser at touchdown zone. Marine Structures 41, 267-287.